Journal of Biotechnology 391 (2024) 92–98

Contents lists available at ScienceDirect

Journal of Biotechnology

journal homepage: www.elsevier.com/locate/jbiotec

Distal mutations enhance efficiency of free and immobilized NOV1 dioxygenase for vanillin synthesis

Mario De Simone [a], Lur Alonso-Cotchico [b], Maria Fátima Lucas [b], Vânia Brissos [a], Lígia O. Martins [a,*]

[a] Instituto de Tecnologia Química e Biológica António Xavier, Universidade NOVA de Lisboa, Av. da República, Oeiras 2780-157, Portugal
[b] Zymvol Biomodeling, Carrer Roc Boronat, 117, Barcelona 08018, Spain

ARTICLE INFO

Keywords:
Biocatalysis
Non-heme iron proteins
Immobilization metal affinity
Lignin valorization
Protein Engineering

ABSTRACT

Protein engineering is crucial to improve enzymes' efficiency and robustness for industrial biocatalysis. NOV1 is a bacterial dioxygenase that holds biotechnological potential by catalyzing the one-step oxidation of the lignin-derived isoeugenol into vanillin, a popular flavoring agent used in food, cleaning products, cosmetics and pharmaceuticals. This study aims to enhance NOV1 activity and operational stability through the identification of distal hotspots, located at more than 9 Å from the active site using Zymspot, a tool that predicts advantageous distant mutations, streamlining protein engineering. A total of 41 variants were constructed using site-directed mutagenesis and the six most active enzyme variants were then recombined. Two variants, with two and three mutations, showed nearly a 10-fold increase in activity and up to 40-fold higher operational stability than the wild-type. Furthermore, these variants show 90–100 % immobilization efficiency in metal affinity resins, compared to approximately 60 % for the wild-type. In bioconversions where 50 mM of isoeugenol was added stepwise over 24-h cycles, the 1D2 variant produced approximately 144 mM of vanillin after six reaction cycles, corresponding to around 22 mg, indicating a 35 % molar conversion yield. This output was around 2.5 times higher than that obtained using the wild-type. Our findings highlight the efficacy of distal protein engineering in enhancing enzyme functions like activity, stability, and metal binding selectivity, thereby fulfilling the criteria for industrial biocatalysts. This study provides a novel approach to enzyme optimization that could have significant implications for various biotechnological applications.

1. Introduction

Vanillin (4-hydroxy-3-methoxybenzaldehyde) is an aromatic compound with a significant share in various industries (Banerjee and Chattopadhyay, 2019; Xu et al., 2024). To meet the growing global demand, currently about 85 % of vanillin is produced by chemical synthesis, which is based on fossil feedstocks and chemical catalysts, while the remaining 15 % is obtained from depolymerization of lignin (Fache et al., 2016). Lignin is a natural and abundant source of phenolic and aromatic compounds, a lignin chemical platform, making lignin-derived vanillin a promising eco-friendly and cost-effective alternative to petroleum-based synthesis through biocatalysis which is gaining popularity daily for eco-friendliness, cost-effectiveness, and long-term sustainability (Hamalainen et al., 2018; Sun et al., 2018). Microbial enzymes such as decarboxylase/oxygenase (Furuya et al., 2017, 2014, 2015; Saito et al., 2020), isoeugenol monooxygenases (Ryu et al., 2013; Yamada et al., 2007a, 2008) and NOV1 dioxygenase (De Simone et al., 2023) were found to convert lignin-derived compounds such as ferulic acid or isoeugenol into vanillin. These enzymes raised interest since they do not require expensive cofactors for catalysis. However, their industrial application is still limited due to a lack of knowledge and low product yields.

In previous studies, we have made progress in understanding the one-step, coenzyme-free conversion of isoeugenol to vanillin by NOV1 dioxygenase (De Simone et al., 2023). This non-heme iron-dependent enzyme catalyzes the cleavage of double bonds of stilbenoid and phenylpropanoid compounds (McAndrew et al., 2016). Advancements in comprehending the structure-function relationships of NOV1 through rational mutagenesis near the active site have been made (De Simone et al., 2023). Furthermore, its potential has been recognized for effectively utilizing lignin-derived intermediates in whole-cell bioprocesses to produce valuable compounds. The biotechnological NOV1 potential

* Corresponding author.
E-mail address: lmartins@itqb.unl.pt (L.O. Martins).

https://doi.org/10.1016/j.jbiotec.2024.06.012
Received 1 April 2024; Received in revised form 11 June 2024; Accepted 13 June 2024
Available online 14 June 2024

was further demonstrated in coupled reactions, where an engineered eugenol oxidase (Guo et al., 2022) first converts lignin-derived 4-*n*-propyl guaiacol (4PG) into isoeugenol, which is subsequently consumed to produce vanillin by a NOV1 improved variant (Maric et al., 2023). This resulted in a vanillin yield of 90 % when starting from synthetically pure 4PG. Furthermore, a substantial 66 % vanillin yield was successfully achieved (Maric et al., 2023), using natural lignin oil containing 27 % 4PG obtained through reductive catalytic fractionation biorefining spruce wood (Renders et al., 2019).

In this study, we have two objectives: 1) use computational tools to predict beneficial mutations distal to active sites, and 2) optimize the immobilization of NOV1 variant enzymes onto solid metal supports by affinity, proposed to be easier and more advantageous over conventional methods of immobilization. Protein engineering is crucial to optimizing enzymes and improving their efficiency and robustness for industrial biocatalysis (Bornscheuer et al., 2019). Most rational and semi-rational designs target residues near the active site or substrate binding sites. Still, it is becoming increasingly clear that distal sites $\geq$ 10 Å significantly contribute to the enzymatic function (Gu et al., 2023; Lee and Goodey, 2011), although the mechanisms underlying their influence are still unclear (Motlagh et al., 2014; Wilding et al., 2019). Current strategies for identifying distal hotspots in enzymes involve assessing the enzyme's conformational landscape to understand its allosteric behavior (Osuna, 2021; Wang et al., 2020), relying on lengthy molecular dynamics simulations. Emerging machine-learning models offer a promising approach to identifying these functional sites (Cagiada et al., 2023). Recently, as part of Zymvol's proprietary software for enzyme engineering Zymevolver (trade secret), Zymspot was validated. This algorithm is able to pinpoint long-range mutations with minimal human intervention, allowing the construction of the so-called smart libraries that made significant time-saving protein engineering (Casilli et al., 2024; Zymvol-Biomodeling). On the other hand, immobilization confers enzyme stabilization, simplifies the separation of products, and enables recycling, enhancing the efficiency and cost-effectiveness of the industrial application of enzymes (Basso et al., 2022; Sheldon and van Pelt., 2013; Winand et al., 2023). While vanillin production using whole cells has been well investigated, there are few reports concern its production using immobilized enzymes which can, nevertheless provide advantages in specific applications (Furuya et al., 2017; Liu et al., 2023). The high costs of the carrier, low immobilization efficiency and loss of activity are common drawbacks of enzyme immobilization (Es et al., 2015). Still, the development of new supports by affinity interaction allows higher immobilization efficiency, faster immobilization, and even the possibility to perform a "one-pot" purification and immobilization with clear advantages over conventional cross-linking, covalent and ionic binding immobilization techniques (Barbosa et al., 2015).

Herein, we employed Zymspot to identify advantageous single distal mutations on the NOV1 scaffold. We generated variants with enhanced catalytic rates and stability compared to the wild-type through site-directed mutagenesis and recombination. Double and triple-mutation-containing variants were selected and immobilized on Chromalite© MIDA/M particles with different metal ions, utilizing their His-tags' metal affinity. These engineered immobilized enzymes outperformed the wild-type in vanillin production, demonstrating significant improvements. Our study highlights the importance of distal interactions in improving enzymatic properties, i.e., the importance of developing strategies for distal-mutation-based protein engineering.

2. Materials and methods

2.1. Bacterial strains, plasmids, and culture media

Escherichia coli strain DH5α (Novagen) was used to amplify plasmid constructs. *E. coli* BL21 star (DE3, Invitrogen) strain was used to express the *nov1* gene cloned in pET-28a (+) plasmid (Novagen) and its variants. In the BL21star strain, the expression of the *nov1* gene is controlled by the T7 promoter and induced by isopropyl β-D-1-thiogalactopyranoside (IPTG). Luria-Bertani medium (LB) was used to grow *E. coli* strains, supplemented with kanamycin (50 μg mL^{-1}).

2.2. Identification of NOV1 distal hotspot residues

Our strategy comprised Zymvol's in-house algorithm, Zymevolver, and its utility to depict distal hotspots, known as Zymspot (Zymvol--Biomodeling). This algorithm deploys bioinformatics and structure-based approaches to depict long-range mutations with the potential to perturb the conformational dynamics of the enzyme, ultimately influencing the population of catalytically productive conformations. It has consistently demonstrated its efficiency in more than 20 enzyme engineering campaigns to improve catalytic properties (mainly activity, selectivity, enzyme stability, operational stability, and expression) in approximately 30 % of the predicted mutant libraries. In this work, it has been used to improve the activity of NOV1 against isoeugenol.

2.3. Construction of nov1 variants using site-directed mutagenesis

Single amino acid substitutions in the *nov1* gene were inserted using the Quick-Change site-directed mutagenesis protocol (Stratagene). The plasmid pET-28a (+) containing the *nov1* gene was used as a template using appropriate primers (Table S1), and the PCRs were performed as previously described (De Simone et al., 2023). The amplified products were purified using GFX PCR DNA and a Gel Band Purification kit (GE Healthcare). The final PCR products were digested with *Dpn*I to eliminate the wild-type template and were used to transform electrocompetent *E. coli* strain DH5α cells. The presence of the desired mutations in the resulting plasmids and the absence of additional inadvertent mutations in other regions of the inset were confirmed by DNA sequencing.

2.4. Recombination by DNA-shuffling

DNA shuffling was performed after amplification of genes coding for variants I222V, L286W, T299S, M324K, L372A and N478S using primers pET21Fwd and pET21Rev (Table S1). A mixture containing 200 ng of each parental gene was digested with 0.04 U of DNase I in 200 mM Tris-HCl, pH 7, with 0.2 M $MnCl_2$ for 10 min at 15°C in a thermal cycler. Digestion was stopped by adding 50 mM EDTA. The PCR reassembly was performed in a 20 μL reaction volume containing 5 μL of DNA fragments, 200 μM of dNTPs, NZYProof polymerase buffer and 2.5 U of NZYProof polymerase. After an initial denaturation period of 3 min at 96 °C, the subsequent steps were repeated for 45 cycles in a thermal cycler: 1 min at 94 °C, 90 s at 59 °C, 90 s at 56 °C, 90 s at 53 °C, 90 s at 50 °C, 90 s at 47 °C, 90 s at 44 °C, 90 s at 41 °C and 1 min + 5 s/cycle at 72 °C followed by a final 10 min period at 72 °C. The PCR reassembly products were amplified by PCR using the primers NOV1-GApET28a Fwd and NOV1GApET28a Rev (Table S1) as previously described (De Simone et al., 2023). The vector pET28a was amplified by PCR using primers pET28aGAnov1 Fwd and pET28aGAnov1 Rev (Table S1) with the following conditions: 50 μL reaction volume containing 2.5 ng of DNA template, 200 μM dNTPs, Q5 polymerase buffer and 2.5 U of Q5® High-Fidelity DNA polymerase (New England Biolabs). After an initial denaturation period of 1 min at 98 °C, the subsequent steps were repeated for 35 cycles in a thermal cycler: 30 s at 98 °C, 20 s at 72 °C, 2 min at 72 °C, followed by a final 10 min period at 72 °C. The amplified products were purified using GFX PCR DNA and Gel Band Purification kit (GE Healthcare, Chicago, IL, USA). The ligation between shuffling products and vector pET28a was performed using the NEBuilder® HiFi DNA Assembly (New England Biolabs). The constructed library was first introduced into E. cloni 10 G ELITE electrocompetent cells (Lucigen), the plasmids were extracted and then propagated in *E. coli* BL21 star cells.

2.5. High-throughput activity screening in 96-well plates

Single colonies were picked from a fresh agar plate and transferred to 96-well microplates containing 200 µL of LB medium supplemented with 50 µg mL^{-1} kanamycin. Cell cultivation, disruption and activity screenings in crude extracts for isoeugenol following vanillin production at 340 nm (ε = 15,97 M^{-1} cm^{-1}) were performed as previously described (De Simone et al., 2023).

2.6. Enzyme production and purification

The cultivation of recombinant *E. coli* BL21star strains in 100 mL LB medium supplemented with kanamycin in 500 mL Erlenmeyer's at 37 °C, 100 rpm shaking and the induction of gene expression with 0.1 mM IPTG and 0.5 mM $(NH_4)_2Fe(SO_4)_2(H_2O)_6$ was performed as previously described (De Simone et al., 2023). The protein purification protocol, using an affinity chromatography HisTrap™ column, and the digestion of the pure protein with SUMO-protease were performed as previously described (De Simone et al., 2023). The purified protein concentration was estimated using the molar absorption coefficient of NOV1 (ε_{280} = 81,930 M^{-1} cm^{-1}) calculated from the protein sequence using the ExPASy Bioinformatics Resource Portal (http://web.expasy.org).

2.7. Apparent steady-state kinetic analysis

The activity dependence on pH was measured using Britton-Robinson buffer (pH 3–11), and the optimal temperature was determined at the temperature range of 10–40 °C. Apparent steady-state kinetic parameters were measured at 340 nm by adding the enzyme to a mixture containing isoeugenol (0.01–4 mM) in 100 mM Tris-HCl, pH 9. Kinetic data were fitted directly to the Michaelis-Menten equation using the Origin® software. All enzymatic assays were performed at least in triplicate.

2.8. Thermodynamic and kinetic stability

Protein unfolding was monitored using a Cary Eclipse spectrofluorometer with an excitation wavelength of 296 nm and recording the fluorescence emission of tryptophan residues at 340 nm as previously described (De Simone et al., 2023). Thermal unfolding was analyzed according to a two-state model N ⇌ U. (Eftink, 1998). Thermal inactivation was studied as previously described (De Simone et al., 2023). In brief, enzyme solutions were incubated at 25 °C in 20 mM Tris-HCl, pH 7.6 and at fixed time intervals, aliquots were withdrawn and tested for activity.

2.9. Immobilization on metal-loaded resin by affinity interaction

Chromalite MIDA/M is a microporous iminodiacetic acid polymethacrylic affinity resin, which can be loaded with divalent transition metals. The purified NOV1 wild-type and variant enzymes 12G2 (M324K/L372A), and 1D2 (I222V/L286W/L372A) were immobilized by affinity interaction on Chromalite™ MIDA/M resins loaded with Ni^{2+} (LS04058-186), Co^{2+} (LS04054-186), Zn^{2+} (LS04057-186), Cu^{2+} (LS04055-186) and Fe^{2+} (LS04056-186), taking advantage of the His-tag of the recombinant enzymes. Resins were first equilibrated, washing twice with 1 mL of 50 mM sodium phosphate, pH 8. The immobilization was performed by incubating 0.1 mg protein/10 mg dry resin in the same buffer at 25 °C, under rotary mixing at 15 rpm (Hybrid Mini 10 incubator) for one hour, in a total volume of 0.5 mL. After immobilization, resins were centrifuged, the supernatants were collected, and the carrier was washed with 0.5 mL of buffer. The total free protein was quantified using the Bradford method, and the amount of enzyme immobilized enzyme was calculated from a mass balance. The immobilization yield (1) was determined to evaluate the immobilization process.

$$Immobilization\ yield(\%) = 100^{*}\left(\frac{P1 - P2}{P1}\right) \quad (1)$$

Where P1 is the initial protein concentration, and P2 is the free protein concentration after immobilization present in the supernatant and washing. The immobilized enzymes were resuspended in 0.5 mL of buffer and used in enzymatic assays to measure the specific activity and compared with that of the free enzyme to calculate the activity yield (2) and immobilization efficiency (3). Assays were performed in 1 mL volume, adding 20–100 µl of immobilized enzyme in 100 mM Tris-HCl buffer, pH 9, containing 2 mM isoeugenol in a 96-deep well plate on a shaker at 1000 rpm at room temperature. Reactions were followed, taking aliquots over time and reading absorbance at 340 nm.

$$Activity\ Yield(\%) = 100^{*}\left(\frac{immobilized\ activity}{initial\ activity}\right) \quad (2)$$

$$Immobilization\ Efficiency(\%) = 100^{*}\left(\frac{Activity\ Yield}{Immobilization\ Yield}\right) \quad (3)$$

The kinetic stability of immobilized enzymes was assessed using 0.3 mg protein on 30 mg Chromalite™ MIDI/M/Ni^{2+} in 50 mM sodium phosphate, pH 8, and incubating at room temperature. Samples are withdrawn, cooled, and tested for activity at appropriate times. Inactivation constants k_{in} and half-life values are calculated as previously described (De Simone et al., 2023).

2.10. Bioconversion of isoeugenol to vanillin by immobilized enzymes

Bioconversions were performed using 1.2 mg of enzyme immobilized on 120 mg of Chromalite™ MIDI/M/Ni^{2+}. Immobilized enzymes were resuspended in 1 mL of 100 mM Tris-HCl, pH 9, with 50 mM isoeugenol. Reaction mixtures were transferred into a flask at room temperature at 10,000 rpm. At specific times, aliquots were withdrawn to quantify vanillin production at 340 nm and calculate the % of substrate conversion (defined as [product]/[initial substrate] * 100). After 24 h, all the reaction mixtures were transferred to an Eppendorf tube and centrifuged for 2 min, at 12,000 rpm, to recover the supernatant. The immobilized enzymes were washed with buffer, centrifuged, and resuspended with fresh reaction mixtures to start new conversion cycles.

2.11. Other methods

The iron content of purified protein samples was determined by colorimetric assay resorting to the chelator TPTZ (2, 4, 6-Tris(2-pyridyl)-s-triazine) (Fischer and Price, 1964).

3. Results and discussion

3.1. Identification of NOV1 distal hotspots

A comprehensive computational screening was performed in NOV1 dioxygenase using Zymspot, aiming to identify positions that increased NOV1 activity against isoeugenol. As a result, 62 distal positions, covering 13 % of the protein, were identified to have a key role in modulating the enzyme properties. This list was shortened to the best-ranked 20 positions, representing 4 % of the protein. Driven by phylogenetic and structural information, the amino acid variability was assessed at each position, resulting in a final list of 41 single-point residues.

3.2. Construction, screening, and characterization of variants

The distal variants (41) resulting from the computational study were constructed using site-directed mutagenesis, and their activity was measured for isoeugenol (Table S2). Twenty enzyme variants had no

Table 1
The apparent steady-state kinetic parameters of NOV1 wild-type and the eleven variants showing the highest activity for isoeugenol. Activity assays were performed using 100 mM Tris-HCl buffer, pH 9, in the presence of 0.01–4 mM isoeugenol at room temperature. Activity values were normalized by mol Fe^{2+}/mol of protein (%). The results are reported as mean ± standard error of three independent experiments. Errors for k_{cat}/K_m were obtained by propagation.

Enzymes	mol Fe^{2+}/mol of protein (%)	k_{cat} (s^{-1})	K_m (mM)	k_{cat}/K_m (M^{-1} s^{-1}) × 10^3
Wild-type	68 ± 5	7.0 ± 0.3	0.6 ± 0.1	12 ± 2
M324K	40 ± 5	33 ± 3	1.7 ± 0.3	20 ± 4
L372A	51 ± 4	30 ± 3	1.9 ± 0.3	16 ± 3
N478S	40 ± 3	26 ± 4	2.5 ± 0.3	11 ± 2
L286W	60 ± 5	23 ± 1	1.6 ± 0.2	15 ± 2
I222V	30 ± 4	23 ± 1	1.9 ± 0.2	12 ± 1
T299S	64 ± 4	21 ± 2	1.3 ± 0.3	16 ± 4
L286V	41 ± 2	17 ± 1	1.5 ± 0.2	12 ± 2
L286I	35 ± 2	13 ± 1	1.0 ± 0.1	13 ± 2
T299V	36 ± 3	11 ± 1	1.0 ± 0.2	11 ± 2
I222L	33 ± 2	4.2 ± 0.3	1.2 ± 0.2	3.5 ± 0.6
M374A	40 ± 3	-	-	5 ± 1

detectable activity, ten showed lower activity than wild-type, and eleven (T299S, L372A, L286V, M324K, L286W, M374A, I222V, N478S, L286I, T299V, and I222L), around 27 % of the library, showed improved activity as compared to wild-type (Fig. S1). Notably, seven of these improved variants are placed in three positions: T299 (2), L286 (3) and I222 (2), suggesting these positions are very permissive to mutations. The eleven variants were purified and characterized. The purified enzyme preparations are partially iron-depleted, displaying approximately 0.5 mol of iron per mol of protein (Table 1), lower amounts as compared to wild-type, as previously observed in our previous studies (De Simone et al., 2023) and with other isoeugenol oxygenases (Ryu et al., 2013; Yamada et al., 2007b). Notably, all variants displayed an increase in k_{cat} up to 4-fold compared to wild-type except I222L and M374A, although the K_m values are generally 2-fold higher (Table 1, Fig. S2).

3.3. Mapping mutations in the NOV1 X-ray structure

The analysis of the NOV1 crystal structure of NOV1 (5J53), show that the six mutations that resulted in the most improved catalytic features are located at distances ≥ 10 Å from the Fe^{2+} cofactor (Fig. 1**A**, Table S3). Except for the mutation M324K that is at the surface, the remaining mutations are placed in the enzyme's core at the second shell of the non-heme cofactor near one of the four iron-coordinating histidines. For example, T299S and L286W are relatively close to H284 (Fig. 1**B**), whereas N478S is near H476 (Fig. 1**C**) at distances around 5 Å. The influence of L372A on H476 is probably mediated through its proximity (4 Å) to E418, a conserved glutamate residue that stabilizes H476 (Fig. 1**C**). Similarly, I222V is only at 4 Å from K169, stabilizing H167 by H-bond (Fig. 1**D**). M324K appears at the walls of the active site entrance tunnel, close to the substrate entrance loops, and can possibly impact the substrate migration pathway (Fig. 1**E**). These mutations, or a combination of mutations (please see below), can modulate the activity and stability of the enzyme.

3.4. Recombination of mutations by DNA shuffling

To combine the best six mutations (I222V, L286W, T299S, M324K, L372A, and N478S) and attempt to further increase the activity towards isoeugenol, the random recombination of genes was performed using DNA shuffling (Stemmer, 1994). This is an excellent *in vitro* gene recombination technique that allows the randomization of gene mutations, concentrating beneficial mutations. It also facilitates the assessment of potential synergistic conformational effects arising from side-chain orientations, which are unpredictable using single-site mutagenesis. After screening a library of 1700 clones for isoeugenol activity, the best 25 variants were selected for re-screening (Fig. S3), and the variants showing 2-fold higher activity than the wild-type were chosen for DNA sequence analysis (Table S4). The two variants with the highest activity were selected for further studies: variant 12G2, harboring mutations M324K and L372A, and variant 1D2, with mutations I222V, L286W, and L372A. Both variants show comparable optimal activity to the wild-type at pH 9 and 28–32 °C (Fig. S4). Notably, these variants showed ~ 7-fold higher k_{cat} than that of the wild-type (Fig. S5, Table 2) and 3-fold the k_{cat} of the best variant (S283F) identified and studied in our previous work (De Simone et al., 2023). The catalytic efficiency is only 2-fold higher than that of the wild-type because the K_m values are 4-fold higher; however, the turnover number (k_{cat}) is considered the most important parameter for biotechnological applications since bioprocesses usually take place at high concentrations of substrate, i.e., the enzyme's activity is not limited by substrate concentration. The other identified single mutations and mutation S283F from our previous study were inserted using site-directed mutagenesis in each of the variants. Still, these substitutions did not increase further the activity (Table S5).

Thermal unfolding and kinetic stability of NOV1 variants were assessed. Assuming the denaturation process as a two-state model native (N) ⇌ unfolded (U) (Eftink, 1998), the apparent melting temperature (T_m) is defined as the temperature at which half of the protein population is in the unfolded state. The T_m of 12G2 and 1D2 variants are comparable to the wild-type (58 ± 1 °C), suggesting the robustness of the enzyme's native structure is maintained (Table 3). The kinetic or operational stability of an enzyme is helpful to evaluate its resistance to inactivation under specific operating conditions, for example, at a given temperature. It is generally expressed as a half-life time ($t_{1/2}$) (Sanchez-Ruiz, 2010). Notably, the study of the kinetic stability at 25 °C showed a half-life time of 50 ± 5 h for 12G2 and 40 ± 5 h for 1D2 (Fig. S6, S7 and Table 3), which were significantly higher than that of the wild-type (1.7 ± 0.4) or of any other studied NOV1 variant (variant S283F shows a half-life of 29 ± 3 h (De Simone et al., 2023)). Our previous results indicated that the primary molecular determinant of NOV1 kinetic stability is the depletion of iron cofactor from the active site during the enzyme incubation at 25 °C. Therefore, the enhanced kinetic stability of both 12G2 and 1D2 variants may result from stabilizing the iron cofactor, hypothetically, like what was observed with S283F, throughout a conformational effect between the distal mutations and the active site.

3.5. Affinity Immobilization of wild-type and variants

In this study, NOV1 wild-type and variants were produced with a SUMO-tag at the N-terminal to promote higher protein solubility and facilitate purification by affinity chromatography. The His-tag allowed binding to Chromalite® MIDA/M resin loaded with Ni^{2+}, Co^{2+}, Zn^{2+}, Cu^{2+} and Fe^{2+} metals (Fig. 2 and Table S6). The long distance between the His-tag and the active site can provide a good orientation for catalysis, eventually resulting in good enzymatic activity and stability compared to other immobilization methods (Basso et al., 2022). The

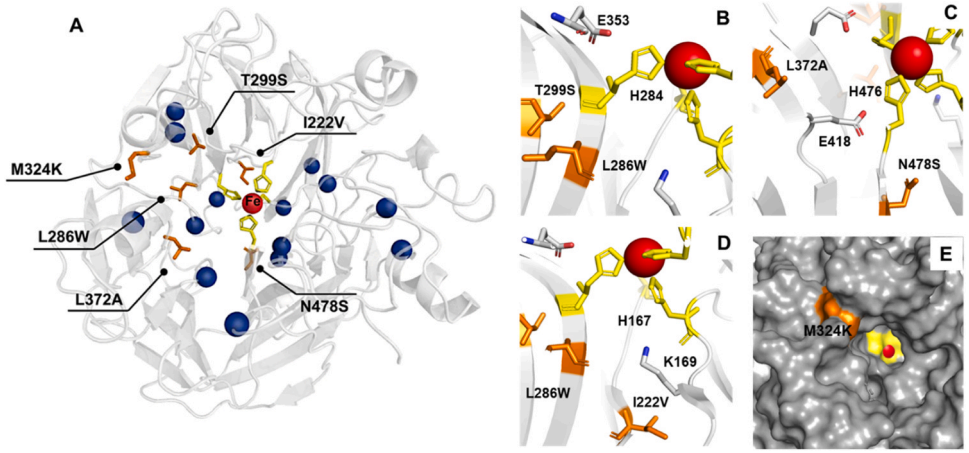

Fig. 1. (**A**) Cartoon representation of NOV1 crystal structure (PDB code 5J53) showing the distribution of hotspots (blue spheres) and the six best hits (in orange). The four iron-coordinating histidines are in yellow, and its surroundings are highlight for H284 in (**B**), H476 in (**C**), and H167 in (**D**). The surface visualization of NOV1 in (**E**) shows the only solvent-exposed mutation M324K located close to the access to the substrate pocket in yellow. Fe^{2+} cofactor is shown as a red sphere.

Table 2
Apparent steady-state kinetic parameters of variants 12G2 and 1D2 that resulted from the recombination of genes using DNA shuffling, measured at room temperature in 100 mM Tris-HCl buffer, pH 9 in the presence of 0.1–4 mM isoeugenol. The results are reported as mean ± standard error of three independent experiments. Errors for k_{cat}/K_m were obtained by propagation.

Enzymes	mol Fe^{2+}/mol of protein (%)	k_{cat} (s^{-1})	K_m (mM)	k_{cat}/K_m (M^{-1} s^{-1}) × 10^3
Wild-type	68 ± 5	7.0 ± 0.3	0.6 ± 0.1	12 ± 2
12G2 (M324K/L372A)	43 ± 4	53 ± 3	2.4 ± 0.3	22 ± 3
1D2 (I222V/L286W/L372A)	50 ± 5	47 ± 3	2.3 ± 0.3	20 ± 3

Table 3
Thermal stability of wild-type and variant enzymes as monitored by thermal inactivation at 25 °C and by fluorescence emission at 330 nm. Half-life at 25 °C is the time after which 50 % of activity is achieved. T_m is the melting temperature at which 50 % of the protein molecules are unfolded. The results are reported as mean ± standard error of three independent experiments for kinetic stability, and two for thermal unfolding.

Enzymes	Half-life at 25 °C (h)	T_m (°C)
Wild-type	1.7 ± 0.4	58 ± 1
12G2 (M324K/L372A)	50 ± 5	58 ± 2
1D2 (I222V/L286W/L372A)	40 ± 5	58 ± 1
L372A	14 ± 2	58
L286W	14 ± 2	56
M324K	4 ± 1	55
T299S	3 ± 1	53
N478S	3 ± 1	55
I222V	3 ± 1	53

immobilization yield (defined as the percentage of protein bound to the resin) was above 80 % for all resins except Fe^{2+}-loaded resin, resulting in the lowest (20–30 %). On the other hand, although the immobilization yield on Cu^{2+} was 99 %, most of the protein is inactive, resulting in the lowest immobilization efficiency (20–40 %). Previous works suggested that different metal ions exhibit varying His-tag selectivity: Cu^{2+} < Ni^{2+} < Co^{2+} < Zn^{2+} < Fe^{2+}, influencing the amount and the way enzymes are immobilized (Basso et al., 2022; Winand et al., 2023). Accordingly, the lower selectivity of resins with Cu^{2+} putatively promotes unspecific interactions with protein surface impairing activity, while the higher selectivity of resins with Fe^{2+} most likely results in a weaker protein binding.

Wild-type and both variants show similar and high immobilization yields in Ni^{2+}, Co^{2+}, and Zn^{2+} loaded resins; however, a significantly higher immobilized activity yield (% of immobilized enzyme activity to initial activity) was measured in variants than in the wild-type.

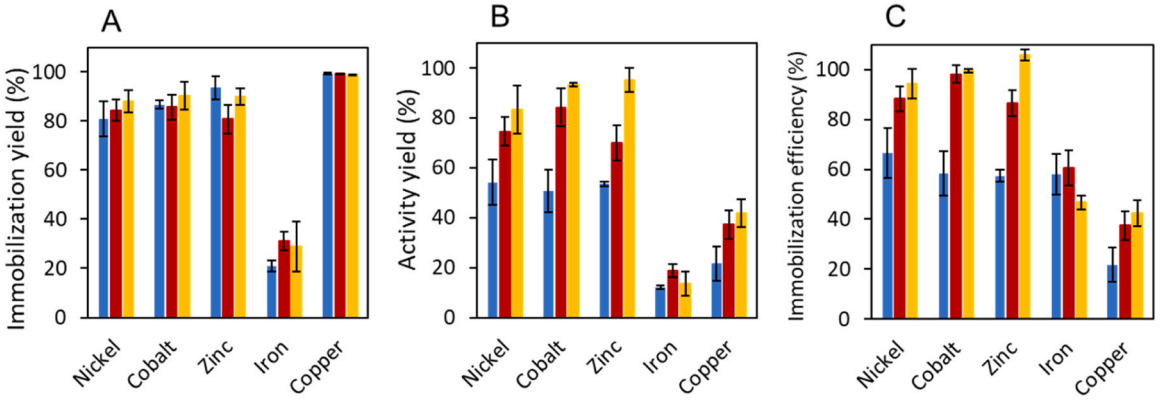

Fig. 2. Immobilization yield (**A**), Activity yield (**B**) and Immobilization efficiency (**C**) of NOV1 wild-type (blue), 12G2 (red), and 1D2 (orange) immobilized onto Chromalite™ MIDA/M loaded with Nickel, Cobalt, Zinc, Iron and Copper metals. The immobilization was performed by incubating 10 mg protein/g resin in 50 mM sodium phosphate buffer pH 8 for 1 h at 25 °C.

Accordingly, the immobilization efficiency (ratio of immobilization yield to immobilization activity) was almost double for the variants (~ 90 %) when compared to the wild-type (~ 50 %). The reduced efficiency of the wild-type can be attributed to its shorter half-life (1.7 ± 0.4 h) under the immobilization conditions (1 h at 25 °C; see Table 3). We increased from 10 mg to 20 mg per gram of resin the protein immobilized (Table S7), observing slightly lower absorption at higher capacities. The stability of enzymes increased after immobilization and storage at room temperature (Fig. S8). The half-life of wild-type increased from 1.7 h (free enzyme) (Table 3) to 32 ± 4 h (immobilized). In contrast, for NOV1 variants immobilization further extended the half-lives to 59 ± 4 h for 12G2, and 57 ± 3 h for 1D2.

3.6. Bioconversion of isoeugenol into vanillin using immobilized enzymes

We tested the recyclability of the immobilization systems by measuring the conversion yields of isoeugenol (50 mM) into vanillin after up to ten reaction cycles of 24 h each (Fig. 3, Table S8). In the first cycle, 1D2 and 12G2 converted 95 % and 62 % of isoeugenol to vanillin, respectively, compared to 38 % for the wild-type. The conversion observed during the first cycle is comparable to and even better than what was observed for whole-cell reaction systems (De Simone et al., 2023; Han et al., 2019; Zhao et al., 2019, 2018). The lower performance of 12G2 compared to 1D2 most likely reflects the lower iron loading (Table 3) and activity immobilization yield (Fig. 2**B**, Table S6). Variant 1D2 maintained the highest conversion along the 10 cycles, producing 164 mM vanillin (~25 mg) at the 1 mL scale, which corresponds to a 33 % molar conversion against the 23 % and 15 % molar conversion of 12G2 and wild-type (Fig. 3, Table S8). However, after the seventh cycle, substrate conversion is residual (< 10 %) for the three enzymes, probably due to enzyme inactivation (Fig. 3). Enzyme immobilization offers advantages over whole-cell reactions by addressing product instability and biosafety, important issues that need to be considered, for example, food application (Liu et al., 2023). The NOV1 1D2 variant immobilized on MIDA/M/Ni^{2+}, produced ~ 4-fold higher amounts of vanillin using lower amounts of protein as compared to a previously reported system using Cso2 oxygenase (De Vitis et al., 2023) immobilized in Sepabeads EC-EA, representing an efficient alternative in the production of vanillin (Furuya et al., 2017).

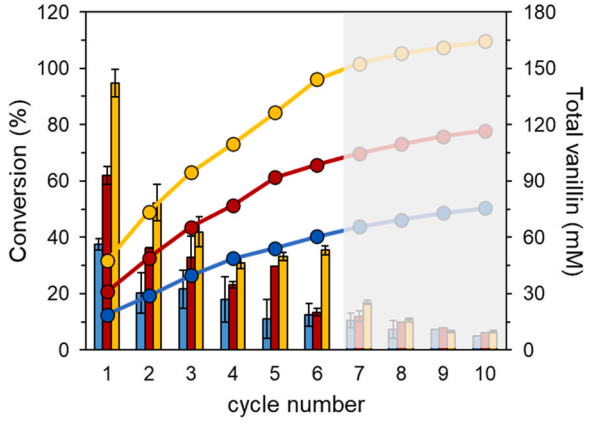

Fig. 3. Isoeugenol conversion to vanillin (%) by immobilized wild-type (blue bars) and variants 12G2 (red bars) and 1D2 (yellow bars) in a 24 h-stepwise 50 mM isoeugenol-addition bioprocess at pH 9 and room temperature. The total amount of vanillin (mM) produced is also shown for wild-type (blue dots), 12G2 (red dots) and 1D2 (blue dots).

4. Conclusion

In summary, this work underscores the importance of distal interactions in enhancing enzymatic properties, emphasizing the value of distal-mutation-based protein engineering strategies. Using the computational tool Zymspot, we identified and mutated 41 distal residues and constructed two variants with two and three distal mutations, achieving nearly a 10-fold increase in activity and up to 40-fold higher operational stability compared to the wild-type. We demonstrated the successful immobilization of these enhanced variant enzymes in MIDA/M/Ni^{2+}. This protocol is straightforward and effective for immobilizing an isoeugenol dioxygenase, providing a higher immobilization efficiency (89–99 %) and conversion yields (95 %) than previously reposted methods. Using these enzymes in reaction mixtures containing 50 mM of isoeugenol, 35 % conversion rates were achieved, after six cycles of reaction, resulting in a total yield of 144 mg vanillin. Our findings provide a proof of concept for the immobilization of computationally optimized enzyme variants, offering significant improvements in both enzyme efficiency and stability. Further development and optimization of these bioprocesses at a larger scale would undoubtedly lead to the economically attractive production of natural vanillin from lignocellulose waste products such as isoeugenol as a precursor.

Funding

This project has received funding from the Bio-based Industries Joint Undertaking (JU) under the European Union's Horizon 2020 Research and Innovation Program under Grant agreement no. 837890. Fundação para a Ciência e a Tecnologia (FCT) additionally supported this work through MOSTMICRO-ITQB R&D Unit (UIDB/04612/2020, UIDP/04612/2020), LS4FUTURE Associated Laboratory (LA/P/0087/2020), and COST-Action COZYME (CA21162) from the European Union are acknowledged for funding networking. MDS acknowledges a Ph.D. grant (2020.08246.BD) from FCT.

CRediT authorship contribution statement

Ligia O Martins: Writing – review & editing, Writing – original draft, Supervision, Resources, Methodology, Investigation, Funding acquisition, Data curation, Conceptualization. **Vânia Brissos:** Writing – review & editing. **Maria Fátima Lucas:** Resources, Conceptualization. **Lur Alonso-Cotchico:** Writing – original draft, Software, Methodology, Investigation, Formal analysis, Conceptualization. **Mario De Simone:** Writing – review & editing, Writing – original draft, Methodology, Investigation.

Declaration of Competing Interest

L. A.-C. is employed by Zymvol Biomodeling S. L. which owns proprietary rights on the algorithm Zymspot used in this study. All authors have read and agreed to the published version of the manuscript.

Data availability

Data will be made available on request.

Acknowledgments

The authors thank Nikola Lončar and Hugo van Beek of GECCO Biotech (Groningen, Netherlands) for providing the Chromalite™ MIDA/M resins loaded with Ni^{2+} (LS04058-186), Co^{2+} (LS04054-186), Zn^{2+} (LS04057-186), Cu^{2+} (LS04055-186) and Fe^{2+} (LS04056-186). Diogo Silva is acknowledged for their help in setting up protocols for enzyme immobilization.

Declaration of Generative AI and AI-assisted technologies in the writing process

During the preparation of this work the authors used ChatGPT OpenAI (version GPT-3.5; https://chat.openai.com/chat and Grammarly (version 8.911.0; https://app.grammarly.com/) to enhance the clarity of the English used. After using these tools/services, the authors reviewed and edited the content as needed and take full responsibility for the content of the publication.

Appendix A. Supporting information

Supplementary data associated with this article can be found in the online version at doi:10.1016/j.jbiotec.2024.06.012.

References

Banerjee, G., Chattopadhyay, P., 2019. Vanillin biotechnology: the perspectives and future. J. Sci. Food Agric. 99 (2), 499–506.

Barbosa, O., Ortiz, C., Berenguer-Murcia, A., Torres, R., Rodrigues, R.C., Fernandez-Lafuente, R., 2015. Strategies for the one-step immobilization-purification of enzymes as industrial biocatalysts. Biotechnol. Adv. 33 (5), 435–456.

Basso, A., Brown, M.S., Cruz-Izquierdo, A., Martinez, C.A., Serban, S., 2022. Optimization of metal affinity ketoreductase immobilization for application in batch and flow processes. Org. Process Res. Dev. 26 (7), 2075–2084.

Bornscheuer, U.T., Hauer, B., Jaeger, K.E., Schwaneberg, U., 2019. Directed evolution empowered redesign of natural proteins for the sustainable production of chemicals and pharmaceuticals. Angew. Chem. Int. Ed. 58 (1), 36–40.

Cagiada, M., Bottaro, S., Lindemose, S., Schenstrom, S.M., Stein, A., Hartmann-Petersen, R., Lindorff-Larsen, K., 2023. Discovering functionally important sites in proteins. Nat. Commun. 14 (1), 4175.

Casilli, F., Canyelles-Nino, M., Roelfes, G., Alonso-Cotchico, L., 2024. Computation-guided engineering of distal mutations in an artificial enzyme. Faraday Discuss.

De Simone, M., Alvigini, L., Alonso-Cotchico, L., Brissos, V., Caroli, J., Lucas, M.F., Monza, E., Melo, E.P., Mattevi, A., Martins, L.O., 2023. Rationally guided improvement of NOV1 dioxygenase for the conversion of lignin-derived isoeugenol to vanillin. Biochemistry 62 (2), 419–428.

De Vitis, V., Cannazza, P., Mattio, L., Romano, D., Pinto, A., Molinari, F., Laurenzi, T., Eberini, I., Contente, M.L., 2023. Caulobacter segnis dioxygenase CsO2: a practical biocatalyst for stilbenoid ozonolysis. Chembiochem 24 (21).

Eftink, M.R., 1998. The use of fluorescence methods to monitor unfolding transitions in proteins. Biochemistry 63 (3), 276–284.

Es, I., Vieira, J.D., Amaral, A.C., 2015. Principles, techniques, and applications of biocatalyst immobilization for industrial application. Appl. Microbiol. Biotechnol. 99 (5), 2065–2082.

Fache, M., Boutevin, B., Caillol, S., 2016. Vanillin production from lignin and its use as a renewable chemical. Acs Sustain. Chem. Eng. 4 (1), 35–46.

Fischer, D.S., Price, D.C., 1964. A Simple serum iron method using the new sensitive chromogen tripyridyl-s-triazine. Clin. Chem. 10 (1), 21–31.

Furuya, T., Miura, M., Kino, K., 2014. A coenzyme-independent decarboxylase/oxygenase cascade for the efficient synthesis of vanillin. Chembiochem 15 (15), 2248–2254.

Furuya, T., Miura, M., Kuroiwa, M., Kino, K., 2015. High-yield production of vanillin from ferulic acid by a coenzyme-independent decarboxylase/oxygenase two-stage process. New Biotechnol. 32 (3), 335–339.

Furuya, T., Kuroiwa, M., Kino, K., 2017. Biotechnological production of vanillin using immobilized enzymes. J. Biotechnol. 243, 25–28.

Gu, J., Xu, Y., Nie, Y., 2023. Role of distal sites in enzyme engineering. Biotechnol. Adv. 63, 108094.

Guo, Y., Alvigini, L., Trajkovic, M., Alonso-Cotchico, L., Monza, E., Savino, S., Maric, I., Mattevi, A., Fraaije, M.W., 2022. Structure- and computational-aided engineering of an oxidase to produce isoeugenol from a lignin-derived compound. Nat. Commun. 13 (1), 7195.

Hamalainen, V., Gronroos, T., Suonpaa, A., Heikkila, M.W., Romein, B., Ihalainen, P., Malandra, S., Birikh, K.R., 2018. Enzymatic processes to unlock the lignin value. Front. Bioeng. Biotechnol. 6, 20.

Han, Z.C., Long, L.K., Ding, S.J., 2019. Expression and characterization of carotenoid cleavage oxygenases from Herbaspirillum seropedicae and Rhodobacteraceae bacterium capable of biotransforming isoeugenol and 4-vinylguaiacol to vanillin. Front. Microbiol. 10 (1869), 1–11.

Lee, J., Goodey, N.M., 2011. Catalytic contributions from remote regions of enzyme structure. Chem. Rev. 111 (12), 7595–7624.

Liu, Y., Sun, L.C., Huo, Y.X., Guo, S.Y., 2023. Strategies for improving the production of bio-based vanillin. Microb. Cell Factor. 22 (1), 147.

Maric, I., Guo, Y.M., Fürst, M.J.L.J., Van Aelst, K., Van den Bosch, S., De Simone, M., Martins, L.O., Sels, B.F., Fraaije, M.W., 2023. A one-pot, whole-cell biocatalysis approach for vanillin production using lignin oil. Adv. Synth. Catal. 365 (22), 3987–3995.

McAndrew, R.P., Sathitsuksanoh, N., Mbughuni, M.M., Heins, R.A., Pereira, J.H., George, A., Sale, K.L., Fox, B.G., Simmons, B.A., Adams, P.D., 2016. Structure and mechanism of NOV1, a resveratrol-cleaving dioxygenase. Proc. Natl. Acad. Sci. USA 113 (50), 14324–14329.

Motlagh, H.N., Wrabl, J.O., Li, J., Hilser, V.J., 2014. The ensemble nature of allostery. Nature 508 (7496), 331–339.

Osuna, S., 2021. The challenge of predicting distal active site mutations in computational enzyme design. WIREs Comput. Mol. Sci. 11 (3), e1502.

Renders, T., Van den Bossche, G., Vangeel, T., Van Aelst, K., Sels, B., 2019. Reductive catalytic fractionation: state of the art of the - biorefinery. Curr. Opin. Biotechnol. 56, 193–201.

Ryu, J.Y., Seo, J., Park, S., Ahn, J.H., Chong, Y., Sadowsky, M.J., Hur, H.G., 2013. Characterization of an isoeugenol monooxygenase (Iem) from Pseudomonas nitroreducens Jin1 that transforms isoeugenol to vanillin. Biosci. Biotechnol. Biochem. 77 (2), 289–294.

Saito, T., Aono, R., Furuya, T., Kino, K., 2020. Efficient and long-term vanillin production from 4-vinylguaiacol using immobilized whole cells expressing Cso2 protein. J. Biosci. Bioeng. 130 (3), 260–264.

Sanchez-Ruiz, J.M., 2010. Protein kinetic stability. Biophys. Chem. 148 (1–3), 1–15.

Sheldon, R.A., van Pelt, S., 2013. Enzyme immobilisation in biocatalysis: why, what and how. Chem. Soc. Rev. 42 (15), 6223–6235.

Stemmer, W.P.C., 1994. DNA shuffling by random fragmentation and reassembly – in-vitro recombination for molecular evolution. Proc. Natl. Acad. Sci. USA 91 (22), 10747–10751.

Sun, Z.H., Fridrich, B., de Santi, A., Elangovan, S., Barta, K., 2018. Bright side of lignin depolymerization: toward new platform chemicals. Chem. Rev. 118 (2), 614–678.

Wang, J., Jain, A., McDonald, L.R., Gambogi, C., Lee, A.L., Dokholyan, N.V., 2020. Mapping allosteric communications within individual proteins. Nat. Commun. 11 (1), 3862.

Wilding, M., Hong, N., Spence, M., Buckle, A.M., Jackson, C.J., 2019. Protein engineering: the potential of remote mutations. Biochem. Soc. Trans. 47 (2), 701–711.

Winand, L., Theisen, S., Lütz, S., Rosenthal, K., Nett, M., 2023. Immobilization of the amidohydrolase MxcM and its application for biocatalytic flow synthesis of pseudochelin A. Catalysts 13 (2), 229.

Xu, L., Liaqat, F., Sun, J., Khazi, M.I., Xie, R., Zhu, D., 2024. Advances in the vanillin synthesis and biotransformation: a review. Renew. Sustain Energy Rev. 189, 113905.

Yamada, M., Okada, Y., Yoshida, T., Nagasawa, T., 2007b. Purification, characterization and gene cloning of isoeugenol-degrading enzyme from Pseudomonas putida IE27. Arch. Microbiol. 187 (6), 511–517.

Yamada, M., Okada, Y., Yoshida, T., Nagasawa, T., 2007a. Biotransformation of isoeugenol to vanillin by Pseudomonas putida IE27 cells. Appl. Microbiol. Biotechnol. 73 (5), 1025–1030.

Yamada, M., Okada, Y., Yoshida, T., Nagasawa, T., 2008. Vanillin production using Escherichia coli cells over-expressing isoeugenol monooxygenase of Pseudomonas putida. Biotechnol. Lett. 30 (4), 665–670.

Zhao, L., Jiang, Y., Fang, H., Zhang, H., Cheng, S., Rajoka, M.S.R., Wu, Y., 2019. Biotransformation of isoeugenol into vanillin using immobilized recombinant cells containing isoeugenol monooxygenase active aggregates. Appl. Biochem. Biotechnol. 189 (2), 448–458.

Zhao, L.Q., Xie, Y.M., Chen, L.Y., Xu, X.F., Zha, C.X., Cheng, F., 2018. Efficient biotransformation of isoeugenol to vanillin in recombinant strains of Escherichia coli by using engineered isoeugenol monooxygenase and sol-gel chitosan membrane. Process Biochem. 71, 76–81.

Zymvol-Biomodeling. Zymspot: a ZYMVOL computational tool for identifying distal mutations. ⟨https://zymvol.com/enzyme-technology/⟩.